Chemical Engineering Journal 428 (2022) 131878

Contents lists available at ScienceDirect

Chemical Engineering Journal

journal homepage: www.elsevier.com/locate/cej

Advanced functional Kevlar composite with excellent mechanical properties for thermal management and intelligent safeguarding

Jianyu Zhou [a], Junshuo Zhang [a], Min Sang [b], Shuai Liu [a], Fang Yuan [a], Sheng Wang [a,*], Shuaishuai Sun [c], Xinglong Gong [a,d,e,*]

[a] CAS Key Laboratory of Mechanical Behavior and Design of Materials, Department of Modern Mechanics, CAS Center for Excellence in Complex System Mechanics, University of Science and Technology of China (USTC), Hefei 230027, China
[b] Department of Chemistry, University of Science and Technology of China, Hefei, Anhui 230026, China
[c] CAS Key Laboratory of Mechanical Behavior and Design of Materials, Department of Precision Machinery and Instrumentation, University of Science and Technology of China, Hefei, Anhui 230027, China
[d] State Key Laboratory of Fire Science, University of Science and Technology of China, 96 Jinzhai Road, Hefei, Anhui 230026, China
[e] Frontiers Science Center for Planetary Exploration and Emerging Technologies, University of Science and Technology of China, Hefei, Anhui 230026, China

ARTICLE INFO

Keywords:
Thermal management
Kevlar fiber
Safeguarding
Shear stiffening gel
MXene

ABSTRACT

Fabric-based personal thermal management devices propel the development of flexible heaters which play important roles in medicinal therapy and protecting humans from cold environments. However, due to the poor mechanical properties, most heaters are easy to be damaged under dynamic loading forces, and also difficult to provide necessary anti-impact protection for human beings. Therefore, it is significant to develop multifunctional fabric heaters with high mechanical properties. Herein, a novel MXene/SSG/Kevlar-based multifunctional textile composite (MS-Kevlar) with sensitive monitoring, thermal management and impact protection is developed by assembling Kevlar fiber, shear stiffening gel (SSG) and two-dimensional MXene. This MS-Kevlar has high sensitive monitoring properties to various stimuli from slight physiological activities to high-speed bullet impact. MS-Kevlar with excellent conductivity shows high thermal management properties which can reach 80.9 °C at 6 V working voltage. Besides thermal protection property, the multifunctional MS-Kevlar can absorb 55.4% force under low-speed impact and still retain the electro-thermal performance after impacted. More importantly, the ballistic limit velocity of MS-Kevlar increases more than 142.1% compared with that of neat Kevlar which could provide safeguarding for humans. Finally, a smart curtain with thermal and anti-impact performance was designed and the based wireless impact alarm system is beneficial for people to assess and avoid dangers.

1. Introduction

Thermal management devices which can convert electricity to heat energy based on the Joule heating effect have be flourished in recent years [1,2]. They show profound applications in personal thermal management [3,4], drug delivery controlling [5,6], defogging and defrosting [7]. Recently, owing to the unique softness, comfort and low price, fabric materials are ideal candidates for developing wearable thermal management devices. So far, fabric-based wearable heater has made profound contribution to personal healthcare which protects human beings from cold weather and frostbite [8–10]. To further improve the electricity-heat conversion efficiency of fabric-based thermal management devices, a novel multifunctional 2D MXene material, with the chemical formula of $M_{n+1}X_nT_x$ [11,12], has been extensively applied due to its unique surface chemistry, ideal metal conductivity and typical layered structure [13–15]. Beside constructing excellent conductive path for high-performance thermal management, introducing 2D MXene also endows wearable thermal devices with other functions. All-in-one wearable flexible heaters with various functions are more favorable in practical thermal protection and therapeutic healthcare.

Zhao et al. fabricate a multifunctional MXene-based smart fabric with fast and stable electro-thermal response for bacterial ablation [16]. The metal-like conductivity of MXene renders the functional fabric high

* Corresponding authors at: CAS Key Laboratory of Mechanical Behavior and Design of Materials, Department of Modern Mechanics, CAS Center for Excellence in Complex System Mechanics, University of Science and Technology of China (USTC), Hefei 230027, China (X Gong and S Wang).
E-mail addresses: wsh160@ustc.edu.cn (S. Wang), gongxl@ustc.edu.cn (X. Gong).

https://doi.org/10.1016/j.cej.2021.131878
Received 20 April 2021; Received in revised form 23 July 2021; Accepted 13 August 2021
Available online 20 August 2021

sensitivity to humidity, which enables to act as wearable respiration monitoring device. Ma et al. prepare a hydrophobic and electrical/photonic/mechanical tri-responsive textile composite by decoration of conductive MXene nanosheets onto air-laid paper [17]. In addition, Liu et al. develop an intelligent PET fabric based on MXene with excellent electromagnetic shielding effect, which not only maintain electro-thermal capability, but also presents significant photo-thermal effect [18]. However, most wearable fabric-based thermal devices can only withstand slight human movements because of its weak mechanics property, such as joint flexion [19], facial expression [20] and pulse [21], etc. The thermal as well as electrical performance of the as-prepared flexible devices are always vulnerable to failure under dynamic impact loading which seriously impede their practical applications.

Harmful collisions such as car crashes and even bullet impacts are widespread all over the world which leads to heavy property damage and human casualties. With the improvement of personal safety awareness, developing wearable devices with force protection performance to protect human beings from danger has become an urgent demand. Due to its high modulus, small fracture strain and low density, Kevlar fibers have been widely used in the protection field [22–24]. Furthermore, shear thickening materials are novel star materials [25–27] and compounding them with Kevlar fibers is proven to be an effective strategy for improving the protective properties of the composite fibers [28–30]. Especially, viscoelastic solid shear stiffening gel (SSG) with typical shear stiffening effect could change its storage modulus by four orders of magnitude under dynamic loading conditions and show fantastic enhancing impact protective effect for Kevlar [31–33]. Due to its excellent mechanical properties, Kevlar is a potential candidate for developing robust wearable thermal management devices. Woven Kevlar-based personal thermal management devices have been fabricated before [34,35]. However, the dynamic mechanical properties of the devices, especially the anti-impact properties under bullet-shooting loading, are always neglected in the past studies. In addition, its thermal stability after the impact excitation have not been explored yet.

In this paper, a wearable thermal management device with multiple functions of force protection, sensing and thermal management is reported based on SSG, Kevlar and lightweight dried MXene. The wearable MS-Kevlar is capable of responding to slight human physical activities and more importantly, it can also capture stimulation from high-speed impact. Under bullet shooting, ballistic limit velocity (v_{bl}) of MS-Kevlar increases at least 142.1%, which shows excellent force safeguarding effect. Because of excellent electrical conductivity of MXene, MS-Kevlar can act as a thermal management device by taking advantage of Joule heating. MS-Kevlar still retains stable heating ability after being impact owing to the excellent enhancement effect from SSG on Kevlar which overcome the weak mechanical properties. Finally, an MS-Kevlar based intelligent curtain not only regulates the indoor temperature but also provides protection for the indoor people. The resistance changes of the curtain under impact can be transmitted remotely to the mobile phone through the Bluetooth module, which enables people to effectively avoid danger. To this end, multifunctional MS-Kevlar shows promising applications in new intelligent wearable systems and safeguard areas.

2. Experiments and characterization

2.1. Materials

Hydroxyl silicone oil and boric acid were purchased from Sinopharm Chemical Reagent Co. Ltd, Shanghai, China. The fabric was the plain-woven aramid Kevlar fabric with areal density of 200 g/m^2, and it was also commercially available. MAX-Ti_3AlC_2 was purchased from 11 technology Co. Ltd, Jilin, China. All the chemical reagents were of analytical purity and used as received without further purification.

2.2. Synthesis of lightweight dried MXene

MXene nanosheets solution was prepared by etching the precursor bulk MAX-Ti_3AlC_2 phase powders. First, the MAX phase powder (Fig. 1a I) reacted with the mixture of hydrochloric acid and lithium fluoride to selectively remove the Al layers and the accordion-like multilayered MXene was obtained (Fig. 1a II). These MXene flakes were then delaminated and separated by ultrasonic and further centrifugal treatment to obtain single-layer MXene suspension (Fig. 1a III). The MXene suspension was dripped into soft PDMS mold. Then, they were put into vacuum freeze drier (Fig. 1a Ⅳ) to sublimate the water and lightweight dried MXene was finally obtained.

2.3. Fabrication of MS-Kevlar

Firstly, the SSG solution with a concentration of 0.67 g/mL was obtained by ultrasonic treating SSG in ethyl alcohol for 3 h at room temperature. Neat Kevlar (Fig. 1b I) was tailored and immersed in SSG solution and dried for six times. Thus, SSG/Kevlar (Fig. 1b II) was obtained. Finally, lightweight dried MXene was pressed on SSG/Kevlar by Teflon film at room temperature to obtain MS-Kevlar (Fig. 1b III). Because of the adhesion of SSG, dried MXene could be stuck on it tightly.

2.4. Characterization

The micro-structures of nano-particles and Kevlar were characterized by SEM (Gemini SEM 500, ZEISS). TEM images of MXene nanosheets were observed on a Field emission transmission electron microscopy (JEM-2100F) with an accelerating voltage of 200 kV. Rheological properties of the polymer matrix were measured by a commercial rheometer (Physica MCR 301, Anton Paar Co., Austria). The tested samples were fixed into cylinders with diameter of 20 mm and thickness of 1 mm. The shear frequency varied from 0.1 Hz to 100 Hz. The electrical properties were measured by the ModuLab Materials Test System (Solartron Analytical, AMETEK Advanced Measurement Technology, Inc., United Kingdom). The safeguarding property of MS-Kevlar was explored by a drop hammer test system. In the high-speed bullet impact experiment, a gas gun was used to fire the bullet. The bullet was 8.0 mm in diameter and 2.0 g in weight. MS-Kevlar with the size of 81.6 $\times$ 81.6 mm^2 was fixed at 15 cm away from the muzzle, so that the velocity attenuation of the projectile at this distance could be ignored. A laser velocimeter was applied to measure the initial velocity (v_i) of a bullet. MS-Kevlar was fixed to a steel frame and the wires from MS-Kevlar were connected with a digital oscilloscope which was used to record separated voltage signals. The damage and residual velocity (v_r) of bullets was recorded by a high-speed video camera. The temperature changes of MS-Kevlar during Joule heating were continuously recorded by a multi-channel thermocouple (DT-3891G, Shenzhen Everbest Machinery Industry Co., Ltd, China). Infrared radiation (IR) thermal images were taken by an infrared camera (ImageIR 8300, InfraTec, Germany). The thermal conductivity of the MS-Kevlar was explored by HotDisk method (TPS 2500 S Hot Disk Thermal Constants Analyzer) and the tested MS-Kevlar was stacked in multiple layers as 10 mm in thickness.

3. Results and discussion

3.1. Preparation and electrical monitoring properties of MS-Kevlar

In this work, the precursor bulk MAX-Ti_3AlC_2 phase powder as the raw material exhibited a multi-layer structure (Fig. S1a). However, 2D single-layer Ti_3C_2Tx nanosheets were successfully prepared after chemical treatment (Fig. S1b-d) and the average thickness of single $Ti_3C_2T_x$ nanosheet was 1.5 nm (Fig. S2). Fig. 2a showed the typical Tyndall scattering effect of the MXene suspension, indicating its satisfactory uniformity and stability. After being freezing dried, the MXene was lightweight (Fig. 2b). And then, MS-Kevlar was prepared by

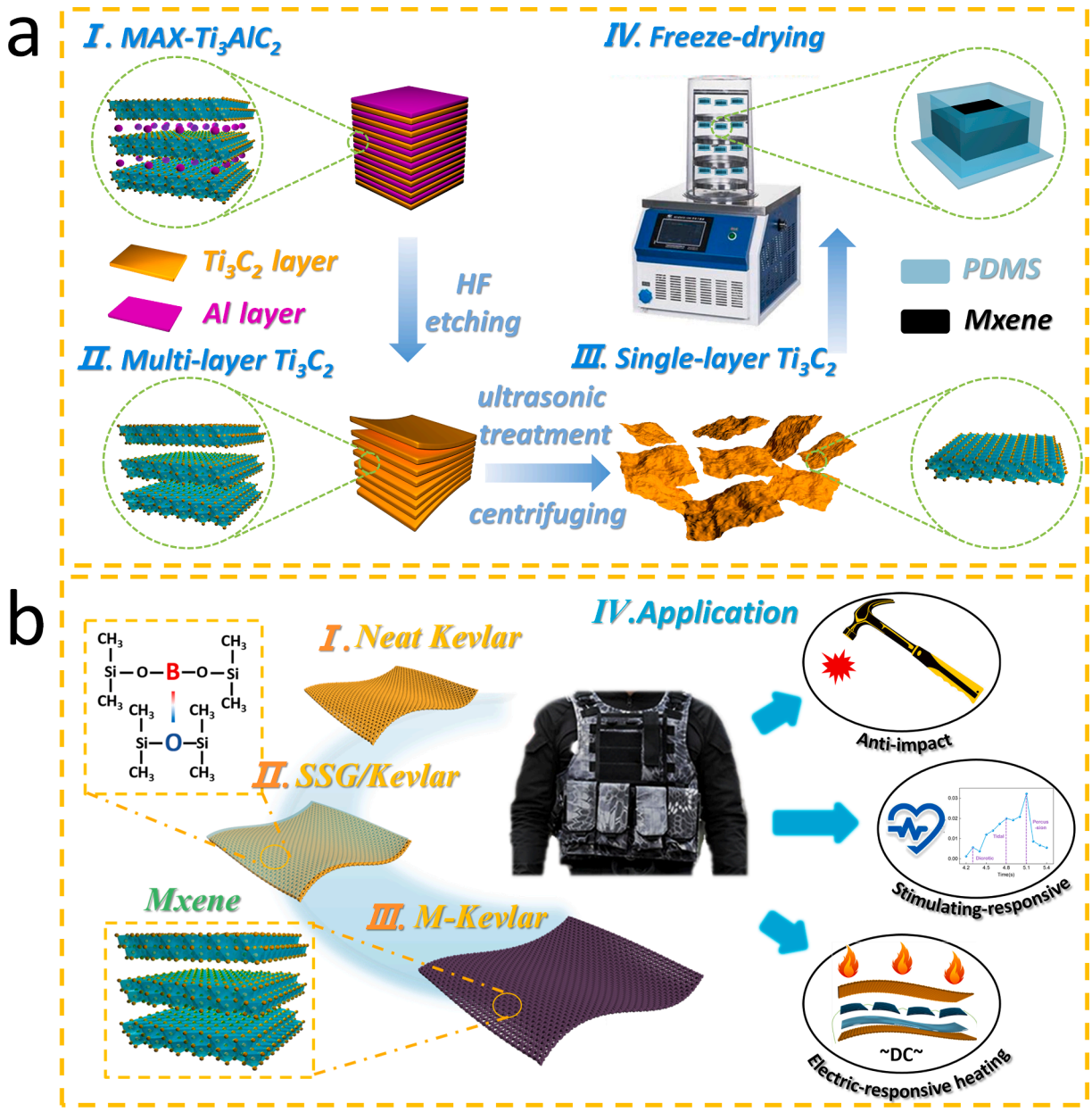

Fig. 1. Schematic of the fabrication process of (a) MXene and (b) MXene/SSG/Kevlar based intelligent fabric (MS-Kevlar).

pressing freezing dried MXene on SSG/Kevlar (Fig. 2c). Besides, bundles of neat Kevlar were smooth and there were small gaps between them (Figs. 2d, S3a). After introducing SSG, the polymer could uniformly attach on Kevlar, forming SSG/Kevlar composite (Figs. 2e, S3b). The mass fraction of SSG on fiber was increased with the increasing of impregnation times until the fiber reached saturation at 7 times (Fig. S3c). In addition, neat Kevlar was loose and easy to deform (Fig. 2f). The introduction of SSG increased the friction between the fibers [36], allowing SSG/Kevlar to maintain shape even under heavy loads (Fig. 2g), while inherited the good flexibility (Fig. 2h).

With the increasing demand for health care and personal safety, MS-Kevlar, as a kind of intelligent fabric, showed a broad application prospect in the wearable device. MXene formed an effective conductive pathway on Kevlar, which endowed the MS-Kevlar with multi-function. When the MXene on SSG/Kevlar was 2 mg, the impedance decreased to 26.5 Ω, the increasing mass was beneficial to the formation of more stable conductive path (Fig. 3a). However, excessive added mass did not significantly improve its conductivity. Thus, 20 mg was chosen as the added mass of MXene on SSG/Kevlar. The stable current–voltage curves (Fig. 3b) indicated the stable resistance of MS-Kevlar with MXene of 20 mg was 3.1 Ω.

MS-Kevlar could respond to throat movements caused by coughing and speech (Fig. 3c). More interestingly, MS-Kevlar showed high sensitivity and three tiny responding peaks corresponding to the “contraction-lifting-relaxing” process of throat deglutition could be observed (Fig. 3d). Meanwhile, MS-Kevlar attached to the wrist also enabled to monitor the pulse condition of human body in real-time which was vital for assessing the heart disease. The characteristic peak positions of the wrist pulse, such as “P” (Percussion), “T” (Tidal), and “D” (Dicrotic) waveforms, could be clearly identified by the sensitive MS-Kevlar (Fig. 3e). “P” and “T” respectively corresponded to the early and late peaks of systolic blood pressure, and “D” appeared in the diastole region [37]. Undoubtedly, the frequency of the pulse dramatically increased after exercising (Fig. 3f). MS-Kevlar worn on fingers could monitor bending angles (Fig. 3g) and maintain good stability (Fig. 3h). Besides, an MS-Kevlar-based sensor array was designed to

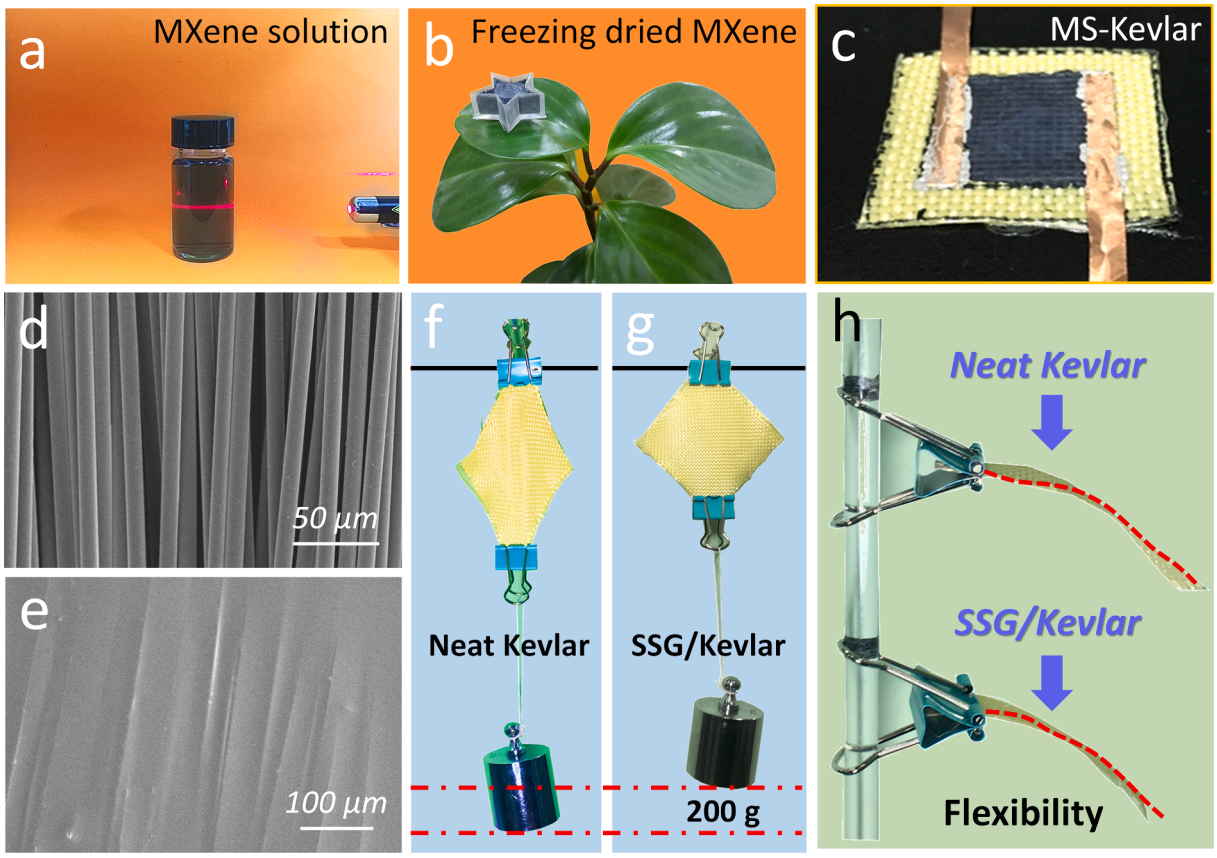

Fig. 2. Optical images of (a) MXene suspension, (b) freeze-drying MXene and (c) MS-Kevlar; SEM images of (d) neat Kevlar and (e) SSG/Kevlar; deformation of (f) neat Kevlar and (g) SSG/Kevlar under 200 g weight load; (h) flexibility of neat Kevlar and SSG/Kevlar.

assess its strain detection properties under external force excitation (Fig. S4), such as falling ball impact (10 g). Since MS-Kevlar was woven from Kevlar fibers, so the strain propagated in the direction of the fiber bundles. Thus, the resistance variation at the cross-region centered around the impact center was the largest (Fig. 3i).

3.2. Joule heating performance of MS-Kevlar based heater

In the past, Kevlar often used in anti-impact areas while ignoring other protection properties. Fortunately, MS-Kevlar with excellent electrical conductivity showed the possibility to protect human body in cold weather based on Joule heating (Fig. 4a). MS-Kevlar based heater was prepared by combining two pieces of copper foil and MS-Kevlar cut into 2 × 2 cm^2. The balance between Joule heating (equal to input power) and heat loss was the decisive factor affecting the saturation temperature of the heating system [38]. Generally, the working process of a heater could be divided into three stages: heating-up, steady-state and cooling-down (Fig. 4b). The heat balance in each stage was expressed as:

$$\begin{cases} cm\cdot\dfrac{dT}{dt} = VI - Q_{cv} - Q_r - Q_{cd} & (Heating-up) \\ 0 = VI - Q_{cv} - Q_r - Q_{cd} & (Steady-state) \\ cm\cdot\dfrac{dT}{dt} = -Q_{cv} - Q_r - Q_{cd} & (Cooling-down) \end{cases} \quad (1)$$

where c, m, T, t, V, I, Q_c ,Q_r and Q_{cd} were specific heat capacity, mass, temperature of the sample, time, input voltage, current, convective heat loss, radiative heat loss and conduction heat loss respectively. The convective heat loss was expressed by

$$Q_{cv} = hA_1(T - T_0) \quad (2)$$

where h, A_1 and T_0 were the convective coefficient, upper surface area of the sample and room temperature (25 °C), respectively. The radiative heat loss could be written as

$$Q_r = \varepsilon\sigma A_1(T^4 - T_0^4) \quad (3)$$

where ε was the surface emissivity of MS-Kevlar varying from 0 to 1 and σ was the Stefan-Boltzmann constant (5.67 × 10^{-8} W m^{-2} K^{-4}), respectively. The conduction heat loss could be written as

$$Q_{cd} = A_2\kappa\frac{dT}{d\delta} \quad (4)$$

where κ, A_2 and $\frac{dT}{d\delta}$ were the heat conductivity lower surface area and temperature gradient, respectively.

In a simplified model for understanding the mechanism of heat exchange (Fig. S5), A was the sum area of the upper and lower surface of MS-Kevlar. In the low-temperature region, the radiative heat loss was much lower than the input power by three orders of magnitude. Therefore, the radiative heat loss was negligible and the second equation of Eq. (1) could be written as:

$$VI = hA_1(T - T_0) + A_2\kappa\frac{dT}{d\delta} \quad (5)$$

which indicated convection and conduction were the major heat loss that influenced the temperature of MS-Kevlar.

According to Eq. (1), higher voltage corresponded to higher saturated temperature. When external voltage reached 10 V, the surface temperature of MS-Kevlar was maintained at 148.6 °C (Fig. 4c, measured by thermocouple). With the increasing of power density, the absolute value of heating-up rate and cooling-down rate also increased (Fig. 4d), which were linearly proportional to the input power,

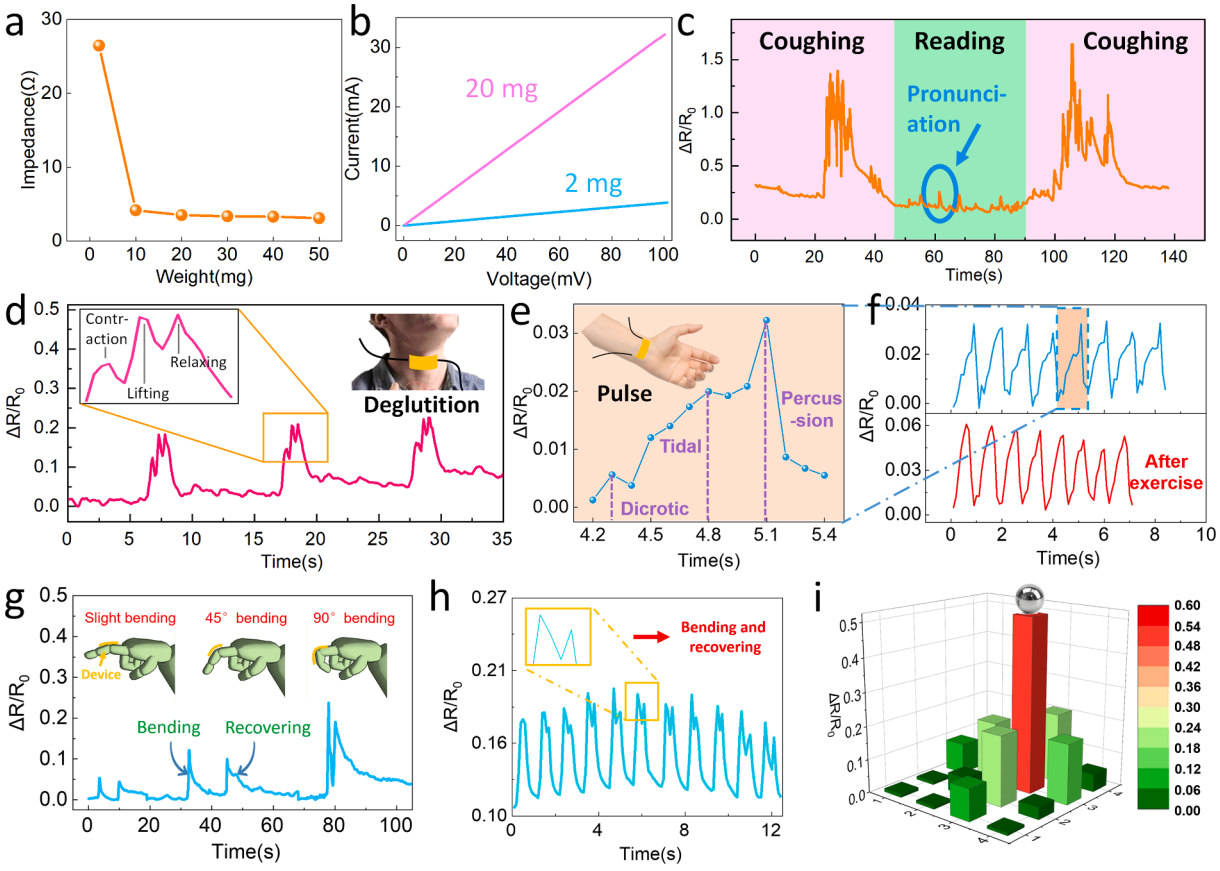

Fig. 3. Applications of MS-Kevlar in detection of small physical signals. (a) The MS-Kevlar impedance as a function of MXene content; (b) current–voltage curves of MS-Kevlar with MXene of 2 mg and 20 mg; the resistance responses under (c) coughing (d) deglutition, (e) wrist pulse, and (g) finger bending; comparison of the (f) pulse vibration before and after exercise; (h) sensing stability under finger bending; (i) recognition of the strain distribution of MS-Kevlar array under a falling ball impact.

respectively (Fig. S6a, b). The saturated temperatures of MS-Kevlar could be precisely adjusted according to the real-time variation of voltage (Fig. 4e) and the temperature gradually increased with the input voltages, which was also recorded by an infrared radiation thermal imaging camera (Insert figure in Fig. 4e).

As a wearable protective device, heating stability of MS-Kevlar-based heater was also vital in practical applications. To evaluate the heating stability and recyclability of the MS-textile wearable heater, the temperature evolution with increasing time at a constant voltage of 5 V was investigated (Fig. 4f). The temperature of heater reached saturation at around 70 °C and maintained steady even after applied external voltage over 3800s, confirming the long-term heating reliability. Furthermore, after 30 times switching cycles, MS-Kevlar-based heater still maintained stable thermal performance (Fig. 4g). The heating stability of MS-Kevlar at different voltages has also been demonstrated in Fig. S7. To this end, the as-designed MS-Kevlar-based heater with good Joule heating performance showed important application in personal thermal protection.

In daily life, exposed conductive layers of wearable electronics showed possible harm to human body and could be easily abraded. Thus, additional protective substrate between the conductive layer and skin was necessary. An MS-Kevlar based wearable wrist band that used Kevlar as the substrate was prepared (Fig. 5a). The MS-Kevlar based heater on the cuff could tightly fit on the skin, which resulted in preventing heat loss and keeping warm. To demonstrate the thermal properties of MS-Kevlar wrist band, temperature-sensitive inks that would change to colorless at 70 °C (Fig. S8) were used. As shown in Fig. 5b I, 4 colorful squares with 2 × 2 cm^2 were drawn. In the squares, there were four letters as "USTC" written by temperature-sensitive inks. When the wrist band was energized, the temperature rose and the "USTC" pattern began to fade (Fig. 5b II). Until reaching 70 °C, the white letters completely appeared on the papers (Fig. 5b III).

To meet the demand in various situation, Kevlar substrate could be replaced by other materials (Fig. 5c). The heating process of heater with different substrate also could be divided into three stages (Fig. 5d). The thermal conductivity of MS-Kevlar was also tested as 0.37 W m^{-1} K^{-1}. Due to varied thermal conductivity, the heater with diverse substrates reached different saturated temperatures after 600s (Fig. 5e). Thus, abundant substrates could be applied in the as-designed heater according to the practical requirement.

3.3. *Anti-impact mechanical performance and simulation under ballistic impact*

Kevlar was widely used in protection due to its properties of lightweight and high mechanical properties. Thus, the anti-impact mechanical performance of MS-Kevlar under ballistic impact was tested by ballistic system presented in Fig. 6a. The bullet was fired from a gas gun launcher, and the v_i (initial velocity of bullet) was changed by controlling the air pressure of the gun. A laser velocimeter connected to an oscilloscope was mounted on the muzzle of the gas gun to measure the v_i of the bullet. The sample was fixed 15 cm away from the muzzle by the bilateral edges clamped. A high-speed video camera was placed behind the composite to record the destruction process and the v_r (the speed which bullet penetrated double-layer Kevlar composite) of the bullet.

The relationship between v_i and v_r was presented in Fig. 6b. The line was fitted by the Recht-Ipson function:

$$v_r = \alpha(v_i^p - v_{bl}^p)^{1/p} \quad (6)$$

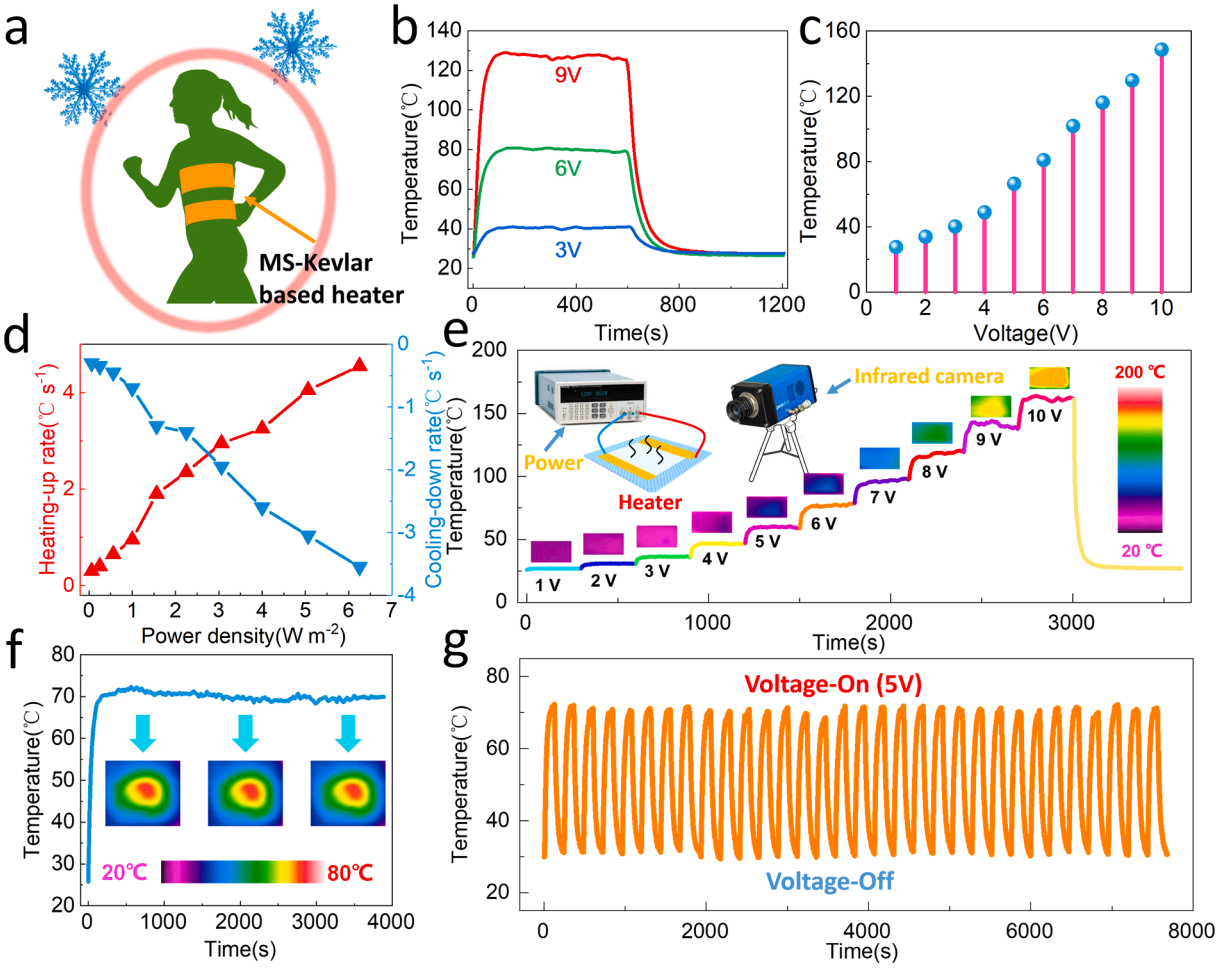

Fig. 4. (a) Schematic of MS-Kevlar based heater; (b) temperature profiles and (c) saturated temperatures at different applied voltages; (d) peak values of heating-up and cooling-down rates as a function of input electrical power density; (e) temperature profiles upon dynamically supplied voltages from 1 to 10 V, insets are the corresponding infrared radiation (IR) thermal images of the heater at different voltages; (f) temperature stability and (g) repeatability of the heater upon repeated supplied voltages of 5 V.

where v_r and v_i were the residual velocity and incident velocity of projectile, α and p were the parameters controlling the shape of curve and v_{bl} (ballistic limit velocity) was the ballistic limit velocity. The fitting curve showed that the v_{bl} of the double-layers neat Kevlar was 80.2 m/s. When the v_i was smaller than v_{bl}, the bullet could not penetrate Kevlar and was bounced. When v_i of the bullet just exceeded the v_{bl}, the v_r increased sharply. However, when the v_i was high enough, relationship between the v_i and the v_r was nearly linear: $v_r \propto v_i$. Moreover, the dissipation energy was defined as:

$$E_{dis} = \frac{1}{2} m(v_i^2 - v_r^2) \tag{7}$$

where E_{dis} and m were the dissipation energy and bullet mass. The initial energy increased, so did the dissipation energy (Fig. 6c).

The destruction process of neat Kevlar (Fig. 6d) and MS-Kevlar (Fig. 6e) was completely recorded by high-speed video camera. When v_i was 129.9 m/s, the bullet could easily penetrate double-layers neat Kevlar. For neat Kevlar, the friction between yarns was small, and the main destruction mode was yarns extraction. (Video S1) More detailed impact processes with different initial velocity was presented in Fig. S9. It was reported that friction between Kevlar yarns significantly increased by impregnating SSG [36]. As a result, the yarns of MS-Kevlar were pulled out difficultly when subjected to impact (Video S2). More yarns were involved in deformation, and the free edge deformed seriously, which caused greater energy dissipated. At the v_i of 194.2 m/s, the double-layers MS-Kevlar was still intact, showing better anti-impact performance.

Gelatin was widely used in ballistic experiments to simulate the human tissue [39,40]. To further explore the excellent anti-impact properties of MS-Kevlar, gelatin (10 × 8 × 7 cm^3) was wrapped in Kevlar. Firstly, the bullet of 105.3 m/s could easily penetrate the gelatin without any protection (Fig. S10a and Video S3). When Kevlar was wrapped around the gelatin, it played a protective role, but the gelatin was still penetrated at 114.3 m/s (Fig. S10b and Video S4). However, when the gelatin was coated with MS-Kevlar, it was infusive that the yarn coupling area was enlarged and the bullet could not lead to penetrating wound at 114.3 m/s (Fig. S10c and Video S5). On the other hand, when neat Kevlar was penetrated, the fibers would be pulled out at high speed, causing serious cuts to the gelatin (Fig. S11a), which increased the risk to the user. This problem was effectively avoided due to MS-Kevlar's strong fiber friction (Fig. S11b).

The Finite Element Method (FEM) results of stress distribution under the same boundary condition were presented in Fig. 7. The interval time for each figure was 10 μs. When the bullet contacted the isotropic Kevlar, the stress wave was traveling at the same speed in the X- and Z-axises. As transmitted to the boundary, the stress wave in the middle fiber bundles perpendicular to the Z-axis would not be accumulated, the stress of the fibers was small, and they did not bear load. The fibers perpendicular to the X-axis were restrained and carried the main load. During the penetration, the middle fiber bundles perpendicular to the Z-

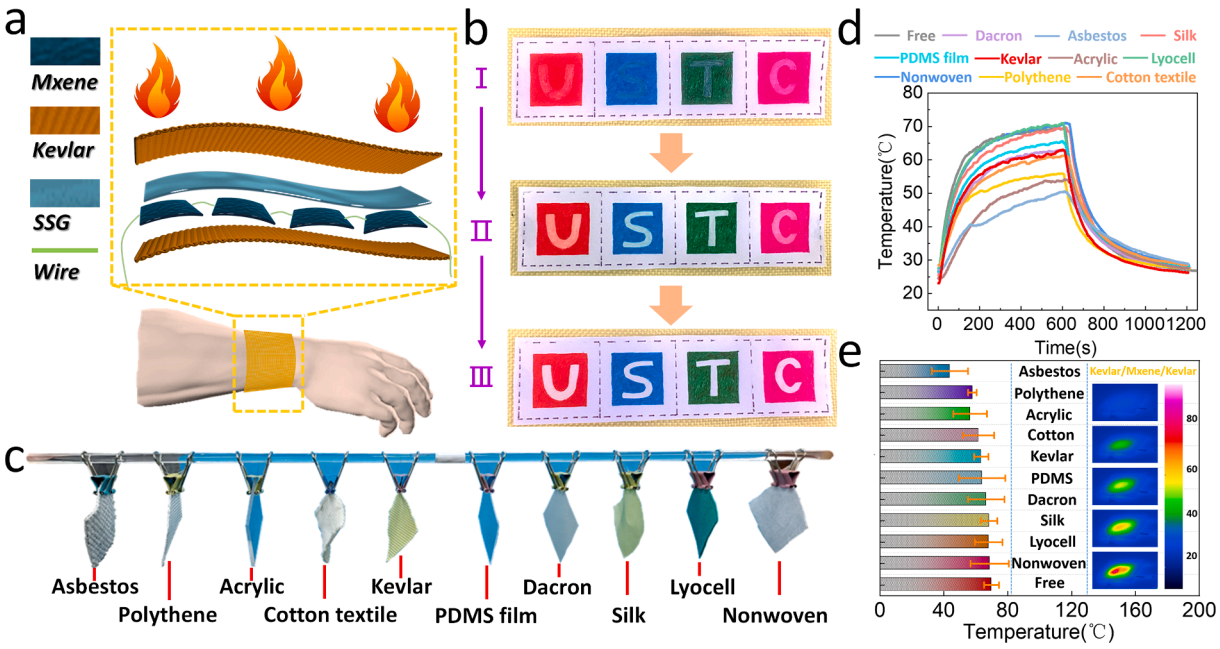

Fig. 5. (a) Schematic of the array of MS-Kevlar based heater; (b) optical images of the pattern drawn by temperature-dependent inks during the heating process; (c) a variety of materials used to cover the MS-Kevlar; (d) temperature profiles and (e) saturated temperatures of MS-Kevlar based heater covered by different materials, insets are the IR thermal images of the MS-Kevlar during heating.

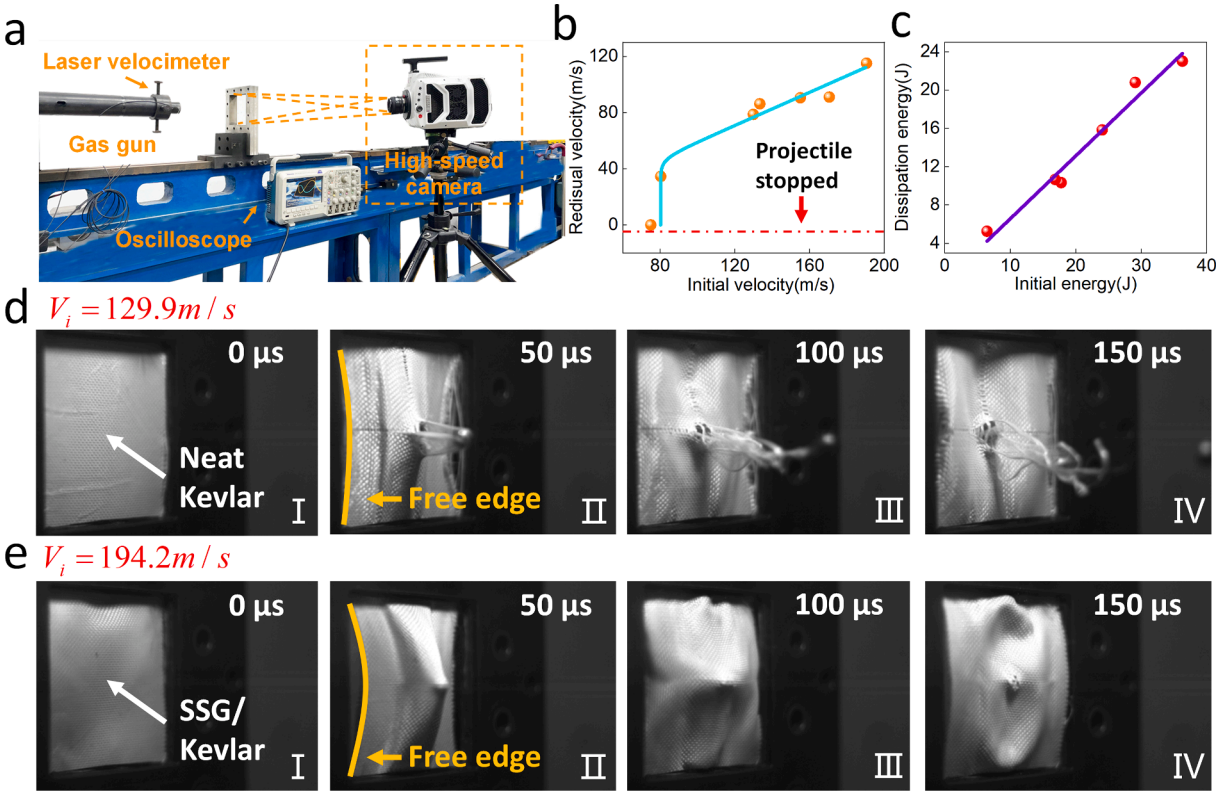

Fig. 6. (a) Optical image of the high-velocity ballistic impact system; (b) the residual velocity results and (c) corresponding energy dissipation results of double layers neat Kevlar; impact process of (d) neat Kevlar at v_i = 129.9 m/s and (e) MS-Kevlar at 194.2 m/s.

axis tended to be pulled out because they were not constrained. The friction between neat Kevlar bundles were low. In the FEM results, the middle fiber bundles were easily pulled out (Fig. S12). However, the friction between the fibers of MS-Kevlar was larger, and the central fiber bundles would not be easily pulled out. Instead, more fiber bundles would deform and dissipate more bullet kinetic energy. Consequently, MS-Kevlar exhibited better anti-ballistic property.

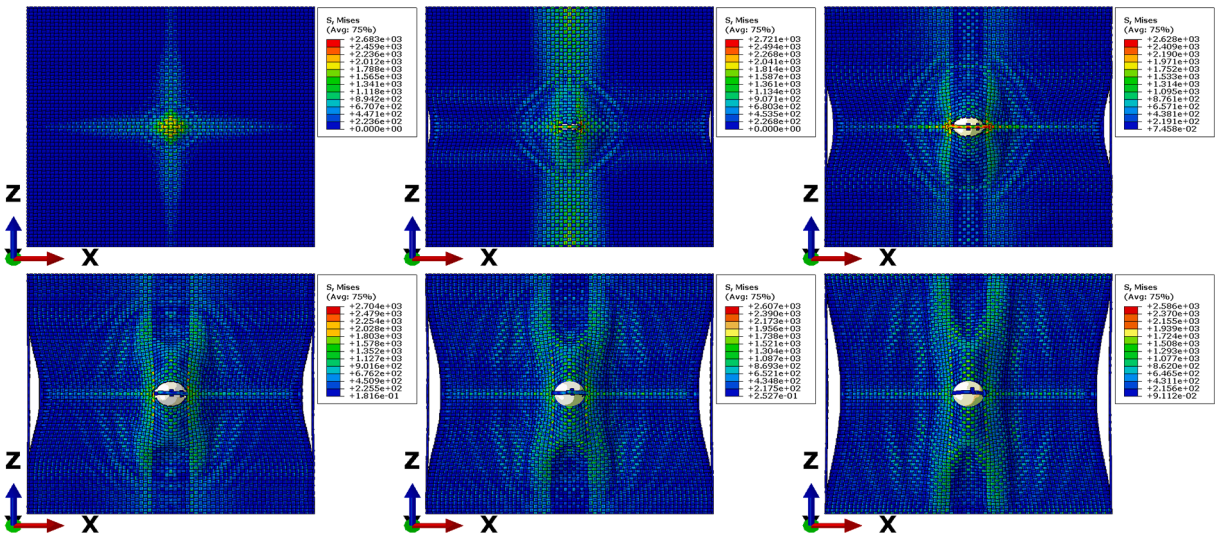

Fig. 7. Simulation results of stress distribution of double layers MS-Kevlar during impact under bilateral edge clamped condition.

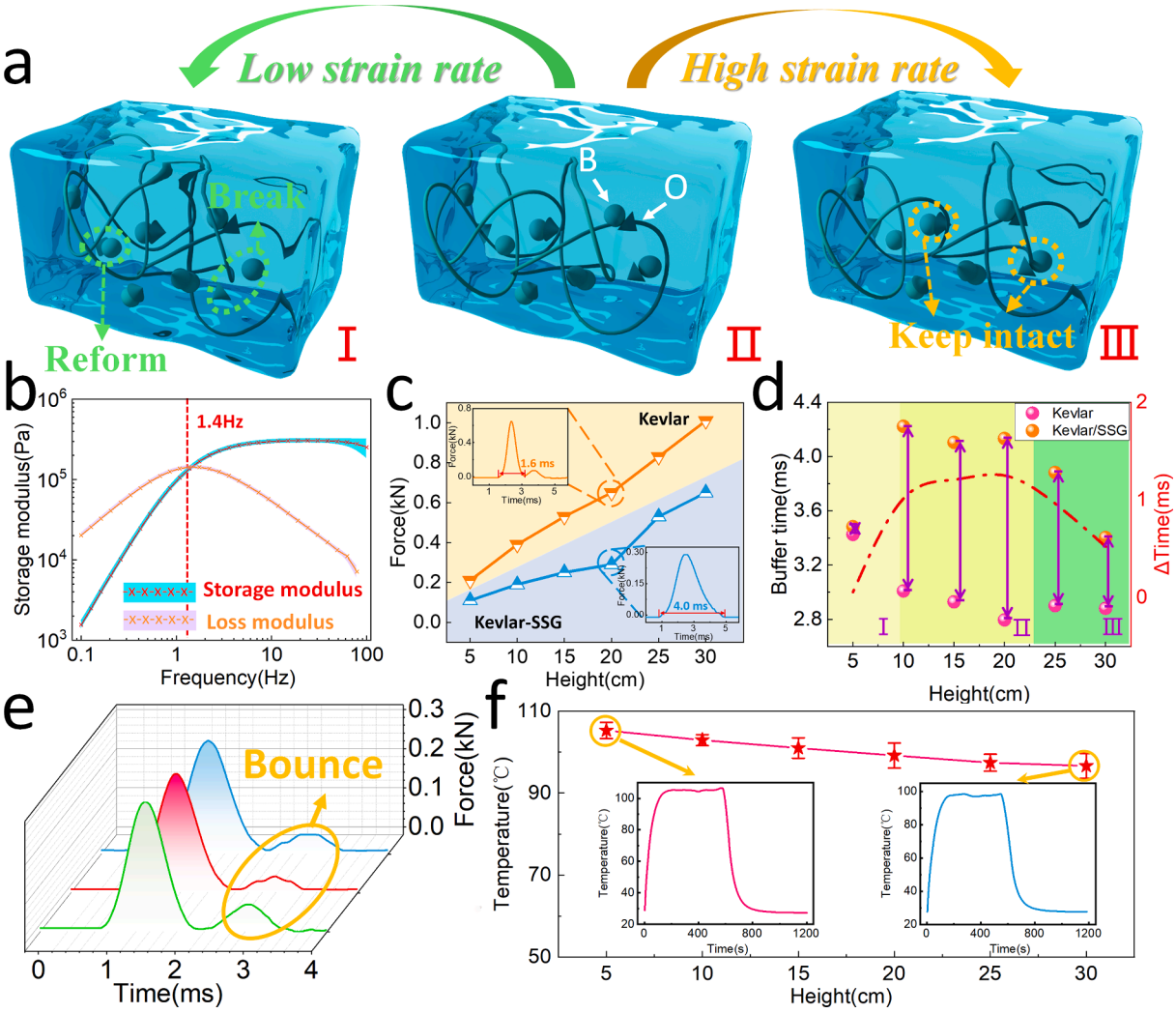

Fig. 8. (a) Mechanism of shear stiffening effect; (b) rheological curve of SSG; dropping height dependent (c) impact force and (d) buffer time of 20 layers MS-Kevlar; (e) impact force cyclic stability loaded from 20 cm; (f) saturated temperatures of impacted MS-Kevlar based heater from different heights.

3.4. Mechanical protection and thermal management properties of MS-Kevlar under dynamic impact conditions

As a functional polymer material, SSG was widely used in intelligent human protection. A mechanism schematic illustration depicting the mechanical behavior of SSG was presented in Fig. 8a. Because of the lack of electrons in the p orbitals of boron atoms and the extra electrons in the oxygen orbitals, there were a large number of dynamic B-O bonds in SSG, (Fig. 8a II). At low strain rates, these cross-links relaxed easily and had enough time to break. On the macro level, SSG showed fluidity and plasticity. In this case, the storage modulus of SSG was low (Fig. 8a I). However, at high strain rates, chemical bonds could not adapt to fast dynamic strain rates in time. So the material behaved as elastic with a significantly increasing storage modulus (Fig. 8a III). Thus, when the shear frequency was 0.1 Hz, the initial storage modulus was 1.5 kPa. As soon as the shear frequency reached 100 Hz, the maximum storage modulus increased to 2.5 MPa, exhibiting typical shear stiffening property (Fig. 8b). Besides, when the shear frequency was lower than 1.4 Hz, the storage modulus was low and the SSG was macroscopically viscous. With the increase of shear frequency, the storage modulus increased and exceeded the loss modulus. Thus, SSG changed from fluid-like to solid-like.

Thanks to the introduction of SSG, MS-Kevlar showed well protection property under low-speed impact conditions. The thickness of the SSG played a critical role in protection performance, thus, the more MS-Kevlar layers assembled, the more force was dissipated (Fig. S13). Take 20 layers of MS-Kevlar as an example, MS-Kevlar could dissipate 55.4% force under low-speed impact (Fig. 8c). In addition, buffer time was an important basis for judging the protection performance [41]. At the falling height of 20 cm, the buffer time increased from 1.6 ms to 4.0 ms (Insert figures in Fig. 8c). Different falling heights would result in different buffer times (Fig. 8d). At low altitudes, the impact velocity was low, so the shear stiffening effect of SSG was not obvious, and the time variation was slight (Fig. 8d I). With the increasing of falling height, shear stiffening effect was gradually obvious (Fig. 8d II). When it reached 30 cm, the energy dissipated by SSG gradually reached the maximum, and the time difference decreased (Fig. 8d III). Besides, the anti-impact property of MS-Kevlar kept stable during several impacts (Fig. 8e). After the harsh impact from 30 cm, the resistance of MS-Kevlar increased. However, due to the protection from SSG, the saturation temperature decreased only 8.2% (Fig. 8f), showing good mechanical-thermal stability under various conditions.

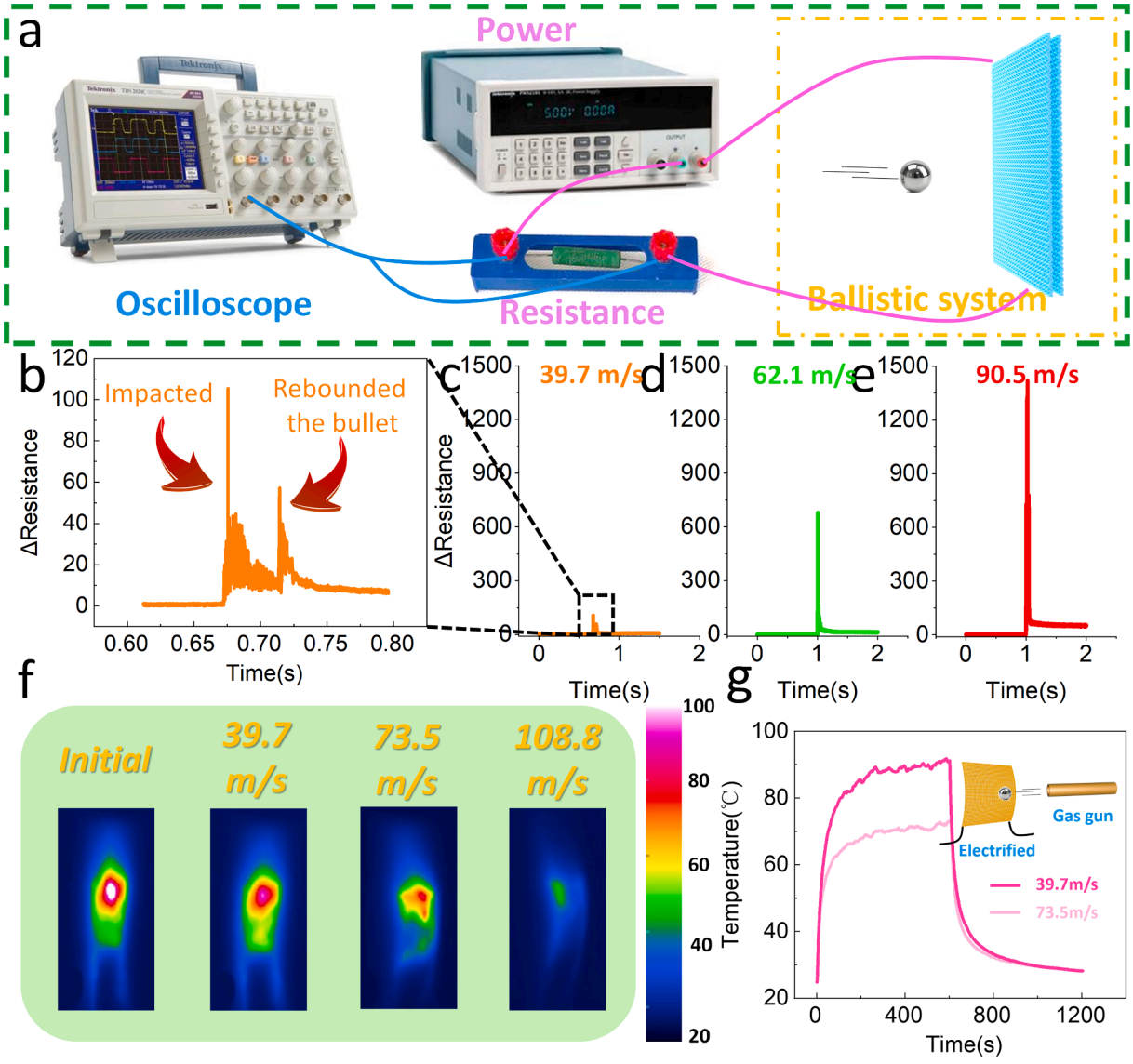

Fig. 9. (a) Schematic of the system for recording the variation of MS-Kevlar resistance during the high-speed impact; the curves of the resistance signal of MS-Kevlar under (b, c) 39.7 m/s, (d) 62.1 m/s and (e) 90.5 m/s; the (f) IR thermal images and (g) temperature profiles of the impacted MS-Kevlar.

In addition, a voltage divided circuit was used in this paper to study the resistance variation of MS-Kevlar during high speed impact (Fig. 9a). MS-Kevlar overlaid with a layer of SSG/Kevlar was connected in series with a constant value resistance, and a programmable power supplier was used to load the voltage. An oscilloscope with sampling rate of 0.1 MHz was connected in parallel to the resistance to measure electrical properties during the impact. The initial resistance of MS-Kevlar was small, and the series resistance shared more voltage. When MS-Kevlar was impacted, the resistance became larger and the shared voltage of the series resistor decreased. The resistance variation of MS-Kevlar during this process could be calculated by

$$R_M = \frac{(U - U_0) \times R_0}{U_0} \tag{8}$$

where R_M, U, U_0 and R_0 were the resistance of MS-Kevlar, total voltage, voltage recorded by the oscilloscope and the resistance of constant value resistance.

When the v_i of bullet was 39.7 m/s, the maximum change of resistance (ΔR) was 105.5 Ω (Fig. 9c). Due to high sampling rate, two peaks were recorded in this process (Fig. 9b). The first peak corresponded to the bullet impacting MS-Kevlar. On account of lower than v_{bl}, bullet was rebounded, which caused the second peak value. With the increasing of v_i, ΔR dramatically changed. When v_i was 62.1 m/s (Fig. 9d) and 90.5 m/s (Fig. 9e), the maximum ΔR was 680.7 Ω and 1418.7 Ω, respectively. Fortunately, because the conductive layer was sandwiched between two layers of SSG/Kevlar, so it could be partially recovered after impact. As shown in Fig. 9f, when external power supply was 7 V, MS-Kevlar could steadily and continuously heat. However, the damage degree of the conductive layer would be more serious with the increase of v_i. At the initial velocity of 39.7 m/s, the heating area was still intact. When v_i was higher than 73.5 m/s, part of the conductive layer was damaged. However, MS-Kevlar also maintain part of its thermal properties at higher impact speeds (Fig. 9g).

3.5. Multi-function curtain based on MS-Kevlar for wireless impact alarm, protection and indoor thermal management

As an innovative material, MS-Kevlar was proven to have excellent mechanical properties and stable electrical properties. Based on this, an intelligent curtain which could take advantage of these merits was developed. The anti-impact property ensured its safeguarding ability, and the electrical conductivity enabled it to realize thermal management and intelligent impact perception. MS-Kevlar could be tailored into different shapes and adapted to windows suitably (Fig. 10a). Occasionally impact or attack from outside may be dangerous for human beings. Precisely judging the danger direction was vital for escaping. Thus, in this work, we developed an impact alarm system by connecting all the MS-Kevlar-based curtains behind windows with Bluetooth module (Fig. 10b). All the resistance variations of curtains under external impact excitation could be transmitted wirelessly to the phone *via* Bluetooth. So people indoors could accurately know the impact position and stay away from the dangerous area in time (Video S3). In addition, MS-Kevlar based multifunctional curtain also showed excellent protection ability (Fig. 10c). When ordinary window glass was impacted by bullets, the high stress led to the rapid expansion of cracks and finally broken the glass (Video S4). At the same time, some sharp glass splashed, which was easy to cause incised wound (Fig. S14a). However, multifunctional curtains behind the windows not only rebounded the bullet (Video S5) but also stopped the splash of broken glass (Fig. S14b). Thus, MS-Kevlar could further prevent the splashing of glass fragments during impact, protecting humans from sharp fragment.

Besides, the multifunctional curtain could play a role in indoor thermal management. When the curtain was electrified, the temperature of the air inside the house rose noticeably (Fig. 10d). FEM could clearly show the indoor thermal management process of MS-Kevlar-based curtain in a confined space. The domain geometry and boundary conditions were shown in Fig. S15. Low and high temperatures were applied to the left and right surfaces respectively. The remaining boundaries (top,

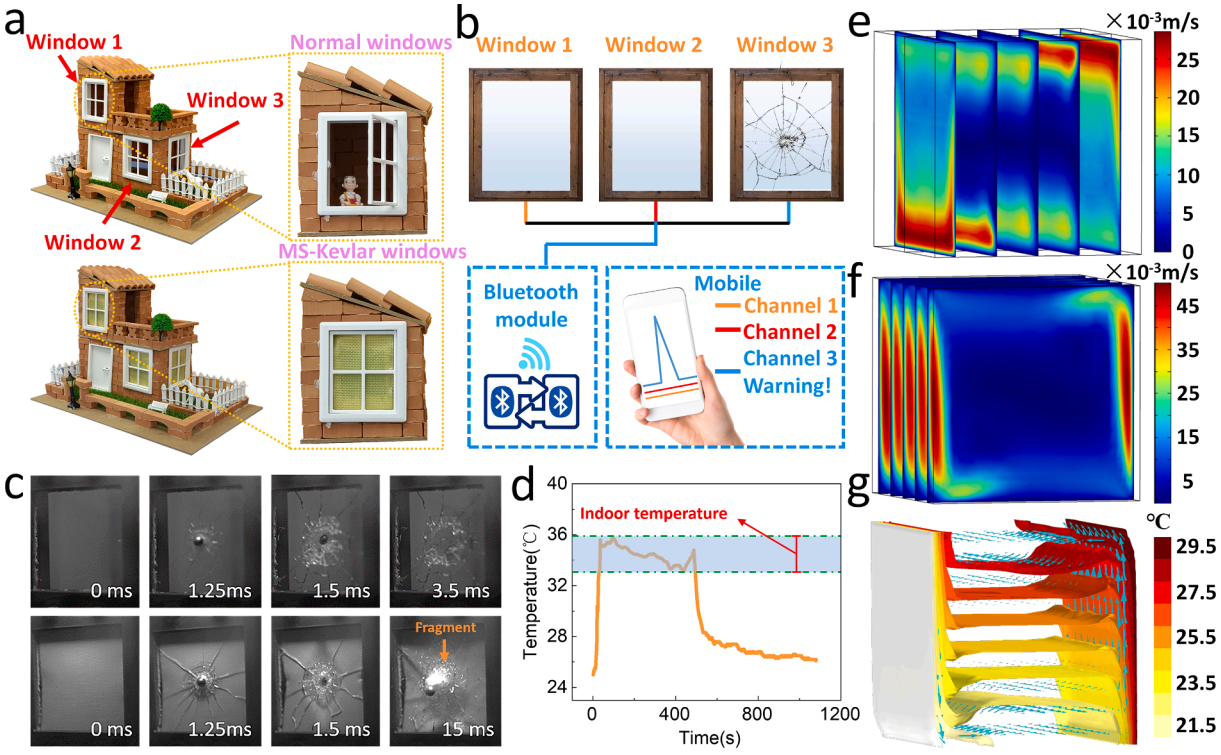

Fig. 10. Schematic of the (a) MS-Kevlar based multifunctional curtains used in home and (b) remote alarm system based on Bluetooth module; (c) impact process of single layer glass and glass with multifunctional curtain behind it; (d) the heating process of the air inside the house when the multifunctional curtain was applied voltage; simulation results of the velocity section which was (e) parallel or (f) perpendicular to the heating plane and (g) isothermal plane during convection process.

bottom, front and back) were thermal insulated. The heat flow velocity section paralleling and perpendicular to the heating plane were presented in Fig. 10e and Fig. 10f, respectively. The faster velocity fields were located at the side boundary. In the process of thermal convection, hot air with low density would rose while the dense cold air located in the bottom layer, resulting in laminar flow phenomenon as shown in Fig. 10g. Interestingly, MS-Kevlar showed great potential for dyeing (Fig. S16a and b) and did not fade after multiple washes (Fig. S16c and d). In general, MS-Kevlar was versatile. It not only provided thermal management of indoor temperature by Joule effect, but also transmitted impacted signals to smart wireless phones to assist users at emergency situations. Thus, MS-Kevlar-based curtains could provide excellent protection for indoor people from impact and cold.

4. Conclusions

This work reported a novel MS-Kevlar composite prepared by combining Kevlar, SSG, and MXene with sensing, force protective, and thermal management properties. As a wearable device that comfortably fit on the body, MS-Kevlar could sense various physiological stimuli. Besides, MS-Kevlar-based heater showed good thermal management property that it could heat stably, and reach 80.9 °C at 6 V external power supply. More importantly, SSG enhanced the bullet-shooting protection of MS-Kevlar by increasing v_{bl} at least 142.1%. FEM method demonstrated that the deformation of yarns and energy dissipation was related to the friction among the yarns. Based on the excellent performance of MS-Kevlar, this paper also developed a new type of bulletproof curtain, which could prevent the damage of bullets and broken glass to indoor personnel. Interestingly, Bluetooth module wirelessly transmitted the resistance signals to mobile phone, helping humans to assess and avoid danger efficiently. Therefore, MS-Kevlar with enhanced mechanical properties showed good application prospects in thermal management devices, wearable sensors and safeguarding fields.

Declaration of Competing Interest

The authors declare that they have no known competing financial interests or personal relationships that could have appeared to influence the work reported in this paper.

Acknowledgment

Financial supports from the National Natural Science Foundation of China (Grant No. 12132016, 11972032, 11802303, 11772320), the Strategic Priority Research Program of the Chinese Academy of Sciences (Grant No. XDB22040502), USTC Research Funds of the Double First-Class Initiative (YD2480002004), the Fundamental Research Funds for the Central Universities (WK2480000009), Hundred Talents Program of Chinese Academy of Sciences - Young Talents (KY2090000067) are gratefully acknowledged.

Appendix A. Supplementary data

Supplementary data to this article can be found online at https://doi.org/10.1016/j.cej.2021.131878.

References

[1] Y. Yao, K.K. Fu, C. Yan, J. Dai, Y. Chen, Y. Wang, B. Zhang, E. Hitz, L. Hu, Three-dimensional printable high-temperature and high-rate heaters, ACS Nano 10 (2016) 5272–5279. https://pubs.acs.org/doi/10.1021/acsnano.6b01059.

[2] Y. Sun, R. Ding, S.Y. Hong, J. Lee, Y.-K. Seo, J.-D. Nam, J. Suhr, MXene-xanthan nanocomposite films with layered microstructure for electromagnetic interference shielding and Joule heating, Chem. Eng. J. 410 (2021) 128348, https://doi.org/10.1016/j.cej.2020.128348.

[3] R. Hu, Y. Liu, S. Shin, S. Huang, X. Ren, W. Shu, J. Cheng, G. Tao, W. Xu, R. Chen, X. Luo, Emerging materials and strategies for personal thermal management, Adv. Energy Mater. 10 (17) (2020) 1903921, https://doi.org/10.1002/aenm.201903921.

[4] Y. Wang, L. Chen, H. Cheng, B. Wang, X. Feng, Z. Mao, X. Sui, Mechanically flexible, waterproof, breathable cellulose/polypyrrole/polyurethane composite aerogels as wearable heaters for personal thermal management, Chem. Eng. J. 402 (2020) 126222, https://doi.org/10.1016/j.cej.2020.126222.

[5] H.u. Tao, S.-W. Hwang, B. Marelli, B.o. An, J.E. Moreau, M. Yang, M.A. Brenckle, S. Kim, D.L. Kaplan, J.A. Rogers, F.G. Omenetto, Silk-based resorbable electronic devices for remotely controlled therapy and in vivo infection abatement, PNAS 111 (49) (2014) 17385–17389, https://doi.org/10.1073/pnas.1407743111.

[6] H. Lee, C. Song, Y.S. Hong, M.S. Kim, H.R. Cho, T. Kang, K. Shin, S.H. Choi, T. Hyeon, D. Kim, Wearable/disposable sweat-based glucose monitoring device with multistage transdermal drug delivery module, Sci. Adv. 3 (2017), e1601314. https://advances.sciencemag.org/content/3/3/e1601314.

[7] L. Veeramuthu, B.-Y. Chen, C.-Y. Tsai, F.-C. Liang, M. Venkatesan, D.-H. Jiang, C.-W. Chen, X. Cai, C.-C. Kuo, Novel stretchable thermochromic transparent heaters designed for smart window defroster applications by spray coating silver nanowire, RSC Adv. 9 (61) (2019) 35786–35796, https://doi.org/10.1039/C9RA06508C.

[8] J. Luo, L. Huo, L. Wang, X. Huang, J. Li, Z. Guo, Q. Gao, M. Hu, H. Xue, J. Gao, Superhydrophobic and multi-responsive fabric composite with excellent electro-photo-thermal effect and electromagnetic interference shielding performance, Chem. Eng. J. 391 (2020) 123537, https://doi.org/10.1016/j.cej.2019.123537.

[9] S. Zhu, M. Wang, Z. Qiang, J. Song, Y. Wang, Y. Fan, Z. You, Y. Liao, M. Zhu, C. Ye, Multi-functional and highly conductive textiles with ultra-high durability through 'green' fabrication process, Chem. Eng. J. 406 (2021) 127140, https://doi.org/10.1016/j.cej.2020.127140.

[10] J. Pan, B. Hao, P. Xu, D. Li, L. Luo, J. Li, Z. Xia, D. Cheng, A. Xu, G. Cai, X. Wang, Highly robust and durable core-sheath nanocomposite yarns for electro-thermochromic performance application, Chem. Eng. J. 384 (2020) 123376, https://doi.org/10.1016/j.cej.2019.123376.

[11] J. Zhang, N.a. Kong, S. Uzun, A. Levitt, S. Seyedin, P.A. Lynch, S.i. Qin, M. Han, W. Yang, J. Liu, X. Wang, Y. Gogotsi, J.M. Razal, Scalable manufacturing of free-standing, strong $Ti_3C_2T_x$ MXene films with outstanding conductivity, Adv. Mater. 32 (23) (2020) 2001093, https://doi.org/10.1002/adma.v32.2310.1002/adma.202001093.

[12] M. Cao, Y. Cai, P. He, J. Shu, W. Cao, J. Yuan, 2D MXenes: electromagnetic property for microwave absorption and electromagnetic interference shielding, Chem. Eng. J. 359 (2019) 1265–1302, https://doi.org/10.1016/j.cej.2018.11.051.

[13] E. Jiao, K. Wu, Y. Liu, M. Lu, H. Zhang, H. Zheng, C.-a. Xu, J. Shi, M. Lu, Robust bioinspired MXene-based flexible films with excellent thermal conductivity and photothermal properties, Compos. A 143 (2021) 106290, https://doi.org/10.1016/j.compositesa:2021.106290.

[14] K. Li, T.-H. Chang, Z. Li, H. Yang, F. Fu, T. Li, J.S. Ho, P.-Y. Chen, Biomimetic MXene textures with enhanced light-to-heat conversion for solar steam generation and wearable thermal management, Adv. Energy Mater. 9 (34) (2019) 1901687, https://doi.org/10.1002/aenm.v9.3410.1002/aenm.201901687.

[15] S. Xu, G. Wei, J. Li, Y. Ji, N. Klyui, V. Izotov, W. Han, Binder-free $Ti_3C_2T_x$ MXene electrode film for supercapacitor produced by electrophoretic deposition method, Chem. Eng. J. 317 (2017) 1026–1036, https://doi.org/10.1016/j.cej.2017.02.144.

[16] X. Zhao, L.-Y. Wang, C.-Y. Tang, X.-J. Zha, Y. Liu, B.-H. Su, K. Ke, R.-Y. Bao, M.-B. Yang, W. Yang, Smart $Ti_3C_2T_x$ mxene fabric with fast humidity response and joule heating for healthcare and medical therapy applications, ACS Nano 14 (7) (2020) 8793–8805, https://doi.org/10.1021/acsnano.0c0339110.1021/acsnano.0c03391.s001.

[17] C. Ma, Q.i. Yuan, H. Du, M.-G. Ma, C. Si, P. Wan, Multiresponsive MXene ($Ti_3C_2T_x$)-decorated textiles for wearable thermal management and human motion monitoring, ACS Appl. Mater. Interfaces 12 (30) (2020) 34226–34234, https://doi.org/10.1021/acsami.0c1075010.1021/acsami.0c10750.s001.

[18] X. Liu, X. Jin, L. Li, J. Wang, Y. Yang, Y. Cao, W. Wang, Air-permeable, multifunctional, dual-energy-driven MXene-decorated polymeric textile-based wearable heaters with exceptional electrothermal and photothermal conversion performance, J. Mater. Chem. A 8 (25) (2020) 12526–12537, https://doi.org/10.1039/D0TA03048A.

[19] Z. Yang, Y.u. Pang, X.-L. Han, Y. Yang, J. Ling, M. Jian, Y. Zhang, Y.i. Yang, T.-L. Ren, Graphene textile strain sensor with negative resistance variation for human motion detection, ACS Nano 12 (9) (2018) 9134–9141, https://doi.org/10.1021/acsnano.8b03391.

[20] C. Wang, X. Li, E. Gao, M. Jian, K. Xia, Q.i. Wang, Z. Xu, T. Ren, Y. Zhang, Carbonized silk fabric for ultrastretchable, highly sensitive, and wearable strain sensors, Adv. Mater. 28 (31) (2016) 6640–6648, https://doi.org/10.1002/adma.201601572.

[21] Y. Zheng, R. Yin, Y.e. Zhao, H.u. Liu, D. Zhang, X. Shi, B. Zhang, C. Liu, C. Shen, Conductive MXene/cotton fabric based pressure sensor with both high sensitivity and wide sensing range for human motion detection and E-skin, Chem. Eng. J. 420 (2021) 127720, https://doi.org/10.1016/j.cej.2020.127720.

[22] V.A. Chatterjee, S.K. Verma, D. Bhattacharjee, I. Biswas, S. Neogi, Manufacturing of dilatant fluid embodied Kevlar-Glass-hybrid-3D-fabric sandwich composite panels for the enhancement of ballistic impact resistance, Chem. Eng. J. 406 (2021) 127102, https://doi.org/10.1016/j.cej.2020.127102.

[23] J. Shiju, F. Al-Sagheer, Z. Ahmad, Thermal mechanical properties of graphene nano-composites with kevlar-nomex copolymer: a comparison of the physical and chemical interactions, Polymers 12 (2020) 2740, https://doi.org/10.3390/polym12112740.

[24] D. Gregori, R. Scazzosi, S.G. Nunes, S.C. Amico, M. Giglio, A. Manes, Analytical and numerical modelling of high-velocity impact on multilayer alumina/aramid fiber

composite ballistic shields: improvement in modelling approaches, Compos. B 187 (2020) 107830, https://doi.org/10.1016/j.compositesb:2020.107830.
[25] P. Sheikholeslami, B. Muirhead, D.S.H. Baek, H. Wang, X. Zhao, D. Sivakumaran, S. Boyd, H. Sheardown, T. Hoare, Hydrophobically-modified poly(vinyl pyrrolidone) as a physically-associative, shear-responsive ophthalmic hydrogel, Exp. Eye Res. 137 (2015) 18–31, https://doi.org/10.1016/j.exer.2015.05.021.
[26] X. Zhang, W. Li, X. Gong, Study on magnetorheological shear thickening fluid, Smart Mater. Struct. 17 (2008), 015051. https://iopscience.iop.org/article/10.1088/0964-1726/17/1/015051.
[27] Y. Liu, J. Peng, K. Zhu, Effects of shear-thinning/thickening nature on the stability of Couette-like flow with uniform crossflow, Acta Mech. Sin. 29 (6) (2013) 806–810. https://link.springer.com/article/10.1007/s10409-013-0092-4.
[28] Z. Tan, W. Li, W. Huang, The effect of graphene on the yarn pull-out force and ballistic performance of Kevlar fabrics impregnated with shear thickening fluids, Smart Mater. Struct. 27 (2018), 075048. https://iopscience.iop.org/article/10.1088/1361-665X/aaca4b.
[29] Q. He, S. Cao, Y. Wang, S. Xuan, P. Wang, X. Gong, Impact resistance of shear thickening fluid/Kevlar composite treated with shear-stiffening gel, Compos. A 106 (2018) 82–90, https://doi.org/10.1016/j.compositesa.2017.12.019.
[30] M.J. Decker, C.J. Halbach, C.H. Nam, N.J. Wagner, E.D. Wetzel, Stab resistance of shear thickening fluid (STF)-treated fabrics, Compos. Sci. Technol. 67 (3-4) (2007) 565–578, https://doi.org/10.1016/j.compscitech.2006.08.007.
[31] F. Yuan, S. Wang, S. Zhang, Y.u. Wang, S. Xuan, X. Gong, A flexible viscoelastic coupling cable with self-adapted electrical properties and anti-impact performance toward shapeable electronic devices, J. Mater. Chem. C 7 (27) (2019) 8412–8422, https://doi.org/10.1039/C9TC01980D.
[32] S. Zhang, S. Wang, T. Hu, S. Xuan, H. Jiang, X. Gong, Study the safeguarding performance of shear thickening gel by the mechanoluminescence method, Compos. B 180 (2020) 107564, https://doi.org/10.1016/j.compositesb:2019.107564.
[33] F. Yuan, S. Liu, J. Zhou, X. Fan, S. Wang, X. Gong, A smart Kevlar-based triboelectric nanogenerator with enhanced anti-impact and self-powered sensing properties, Smart Mater. Struct. 29 (12) (2020) 125007, https://doi.org/10.1088/1361-665X/abaf08.
[34] A. Hazarika, B.K. Deka, DoYoung Kim, H.E. Jeong, Y.-B. Park, H.W. Park, Woven kevlar fiber/polydimethylsiloxane/reduced graphene oxide composite-based personal thermal management with freestanding Cu-Ni core-shell nanowires, Nano Lett. 18 (11) (2018) 6731–6739, https://doi.org/10.1021/acs.nanolett.8b02408.
[35] A. Hazarika, B.K. Deka, C. Jeong, Y.-B. Park, H.W. Park, Biomechanical energy-harvesting wearable textile-based personal thermal management device containing epitaxially grown aligned Ag-Tipped-NixCo1-xSe nanowires/reduced graphene oxide, Adv. Funct. Mater. 29 (31) (2019) 1903144, https://doi.org/10.1002/adfm.v29.3110.1002/adfm.201903144.
[36] C. Zhao, Y. Wang, S. Cao, S. Xuan, W. Jiang, X. Gong, Conductive shear thickening gel/Kevlar wearable fabrics: a flexible body armor with mechano-electric coupling ballistic performance, Compos. Sci. Technol. 182 (2019) 107782, https://doi.org/10.1016/j.compscitech.2019.107782.
[37] Y. Cheng, Y. Ma, L. Li, M. Zhu, Y. Yue, W. Liu, L. Wang, S. Jia, C. Li, T. Qi, J. Wang, Y. Gao, Bioinspired microspines for a high performance spray $Ti_3C_2T_x$ MXene-based piezoresistive sensor, ACS Nano 14 (2) (2020) 2145–2155, https://doi.org/10.1021/acsnano.9b08952.
[38] Z. Li, Z. Xu, Y. Liu, R. Wang, C. Gao, Multifunctional non-woven fabrics of interfused graphene fibres, Nat. Commun. 7 (2016) 13684. https://www.nature.com/articles/ncomms13684.
[39] A.L. Collins, J.W. Addiss, S.M. Walley, K. Promratana, F. Bobaru, W.G. Proud, D. M. Williamson, The effect of rod nose shape on the internal flow fields during the ballistic penetration of sand, Int. J. Impact Eng. 38 (2011) 951–963. https://www.sciencedirect.com/science/article/pii/S0734743X11001229?via%3Dihub.
[40] J. Zhang, N. Yoganandan, F.A. Pintar, T.A. Gennarelli, Temporal cavity and pressure distribution in a brain simulant following ballistic penetration, J. Neurotraum 22 (2005) 1335–1347. https://www.liebertpub.com/doi/10.1089/neu.2005.22.1335.
[41] S. Wang, L. Gong, Z. Shang, L.i. Ding, G. Yin, W. Jiang, X. Gong, S. Xuan, Novel safeguarding tactile e-skins for monitoring human motion based on SST/PDMS-AgNW-PET hybrid structures, Adv. Funct. Mater. 28 (18) (2018) 1707538, https://doi.org/10.1002/adfm.v28.1810.1002/adfm.201707538.